

MACHINING FORCES FOR ELLIPTICAL VIBRATION-ASSISTED MACHINING¹

D. E. Brehl, M.A. Cerniway, T.A. Dow, and N. Negishi
Precision Engineering Center
North Carolina State University
Raleigh, North Carolina, USA

INTRODUCTION

In “elliptical vibration-assisted machining” (EVAM), a single-point diamond tool is driven in a tiny ellipse at high frequency. This tool tip motion is superimposed on the principal upfeed motion of the workpiece. An important benefit of EVAM is that machining forces are significantly reduced compared to conventional diamond machining. Most reports of EVAM tool forces are average values for an entire vibration cycle since systems typically operate at ultrasonic frequencies and sampling rates of several hundred KHz are thus required to measure force variation within an individual cycle. A reduction in average tool forces can be expected for EVAM simply because the tool separates from the workpiece for a portion of each elliptical cycle. To measure forces within a vibration cycle, Moriwaki and Shamoto [1] used a research unit that operated at 0-10 Hz. This system was run without lubricant inside the vacuum chamber of a scanning electron microscope (SEM), so that secondary causes of tool force reduction—such as improved lubricant penetration to the rake face—were eliminated. As illustrated in Figure 1, the instantaneous as well as the average cutting (principal) and thrust forces in EVAM were shown to be smaller than the conventional machining forces.

Observing that the thrust force in Figure 1 is negative during part of each cutting cycle, Moriwaki and Shamoto argued that in EVAM the upward motion of the tool helps to pull the chip out of the workpiece. Thrust force reversal acts to change the effective shear angle for chip formation, leading to reduced cutting force.

The authors contend that tool force reduction in EVAM derives from the geometry of overlapping successive elliptical toolpaths. In EVAM the chip thickness is established by the overlap between tool passes, and the maximum chip thickness is less than or equal to the depth of

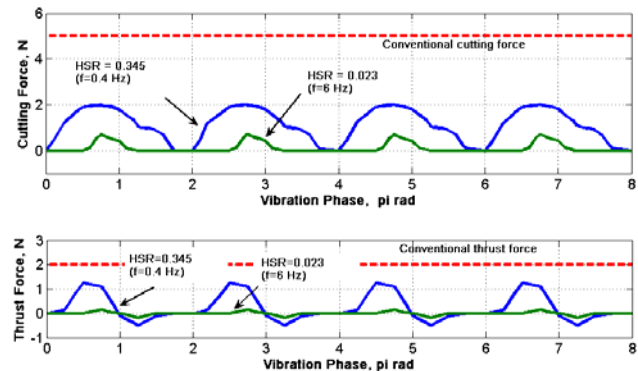


FIGURE 1. Comparison between cutting (top) and thrust forces (bottom) for EVAM and conventional precision machining. Note force reduction grows more marked with increasing horizontal speed ration HSR. Redrawn from [1].

cut, which determines the uncut chip thickness for conventional machining. In EVAM the tool makes many small chips, and executes many passes at lower tool force in a specified time interval. In conventional machining the tool travels a much shorter distance with higher force. For the same volumetric material removal, the work performed by EVAM is therefore consistent with that of conventional machining.

In the current research, a tool force model originally developed for steady-state conventional diamond machining is modified to consider the transient in EVAM. Included are the effect of varying chip thickness, variation in tool contact surface area and of progressively increasing negative rake angle during the machining cycle. Theoretical tool force predictions are verified against experimental data obtained using the Ultramill, an EVAM tool developed by at North Carolina State University. Figure 2 shows the Ultramill concept. Sinusoidal voltage signals, with a phase difference between them, are applied to parallel piezoelectric actuator stacks. A toolholder is driven by the

¹ This paper was written as part of work supported by NSF grant DMI-0423315, monitored by G. Hazelrigg.

stacks, acting a linkage to convert their reciprocating motion into elliptical tool tip motion.

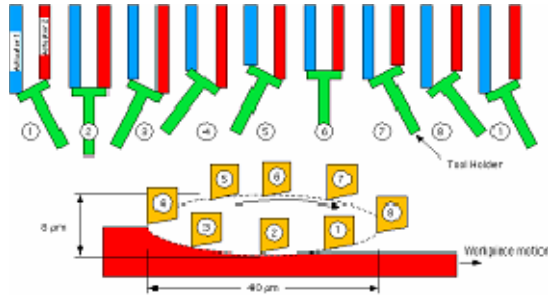


FIGURE 2. Ultramill EVAM concept

EVAM DESCRIPTION

In EVAM the position at time t of the tool tip can be described by

$$X(t) = A * \cos(2\pi * f * t) + V * t \quad (1)$$

$$Z(t) = B * \sin(2\pi * f * t) \quad (2)$$

where $X(t)$ and $Z(t)$ are the instantaneous tool tip positions in the upfeed and depth of cut directions, V is the upfeed velocity of the work material, f is the tool vibration frequency, and A and B are respectively the semi-major axis (X -direction amplitude) and semi-minor axis (Z -direction amplitude) for the machining ellipse.

An EVAM cycle can be characterized by three parameters. The “upfeed index” F_{UP} (Eq. 3) is the distance traveled by the tool relative to the

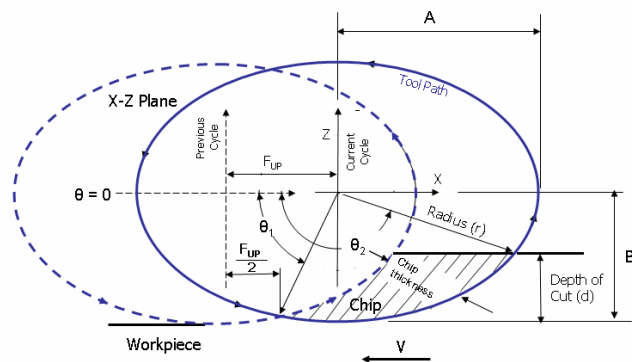


FIGURE 3. EVAM cycle. Two successive cutting passes are approximated by overlapping ellipses. Maximum chip thickness is less than or equal to depth of cut, contributing to reduced tool forces (Z-axis scale is exaggerated compared to X).

work in one cycle. The “horizontal speed ratio” HSR (Eq. 4) relates the peak cutting speed of the tool to the upfeed velocity.

$$F_{UP} = \frac{V}{f} \quad (3) \quad HSR = \frac{V}{2\pi f * A} \quad (4)$$

Small values of F_{UP} and HSR lead to low theoretical surface roughness. The third characterizing parameter, “duty cycle”, is the fraction of each cycle the tool is cutting. Duty cycle becomes larger with increasing HSR and also with increasing ratio of depth of cut, d , to the ellipse vertical amplitude B .

The workpiece upfeed motion means that relative to the workpiece, the toolpath is distorted from a true elliptical shape. When the horizontal speed ratio is small ($HSR < 0.1$), the toolpath can be accurately approximated by overlapping ellipses spaced at intervals of F_{UP} as shown in Figure 3

Chip geometry is affected by the ratio of depth of cut, d , to the ellipse vertical amplitude B . When $d/B \leq 1$, the tool exits the workpiece before completing its elliptical pass and small discontinuous chips are produced. Figure 4a. When $d/B > 1$ the chip remains attached to the workpiece and a long discontinuous chip is produced with small attached segments regularly spaced at intervals of F_{UP} .

TOOL FORCE MODEL

For small crossfeed rates, operations such as turning, facing and raster machining approximate orthogonal cutting. In this situation there are two tool forces, the cutting (or principal) force and the thrust force. These tool forces each can be considered as having two components. The first consists of the forces associated with plastic deformation required to form the chip. The second component consists of friction forces between the tool and workpiece. In both traditional and precision diamond machining, friction arising from contact between the chip and engaged portion of the tool rake face is a major portion of the thrust force. In precision diamond machining, the depth of cut is small relative to the dimensions of tool features such as the cutting edge radius and flank wear land, so that the friction forces associated with these features are significant additions to the thrust and cutting forces

Arcona [4] developed a model for single-point diamond turning which gives machining forces in terms of material properties, chip geometry, tool contact area, and material shear angle:

$$F_C(t) = \frac{H * a_C(t)}{3} * \left[\frac{\cot(\varphi(t))}{\sqrt{3}} + 1 \right] + \mu_F * \sigma_F * a_F(t) \quad (5)$$

$$F_T(t) = \mu * \left[\frac{H * a_C(t)}{3} * \left(\frac{\cot(\varphi(t))}{\sqrt{3}} + 1 \right) \right] + \sigma_F * a_F(t) \quad (6)$$

$$\sigma_F = 0.62 H * \sqrt{\frac{0.43 H}{E}} \quad (7)$$

where $F_C(t)$ and $F_T(t)$ are respectively the instantaneous cutting and thrust forces, $a_C(t)$ is the instantaneous cross-section area of the uncut chip, H is the material surface hardness, E is the material elastic modulus, μ is the friction coefficient between the tool rake face and chip, and $\varphi(t)$ the instantaneous shear angle of the chip. The "friction area" between the tool and the work, $a_F(t)$, consists of the contact area of the cutting edge radius between the rake face and flank face, the area of the wear land behind the edge radius, and the region where elastic springback causes material to contact the flank face after being passed over by the tool. These regions are shown in Figure 4. It is readily seen that for a worn tool the friction area $a_F(t)$ will be larger than for a sharp tool, since cutting edge radius and/or the flank wear land length will be greater. The variables μ_F and σ_F are, respectively, the coefficient of friction for the friction area and the average normal stress in the material arising from elastic behavior.

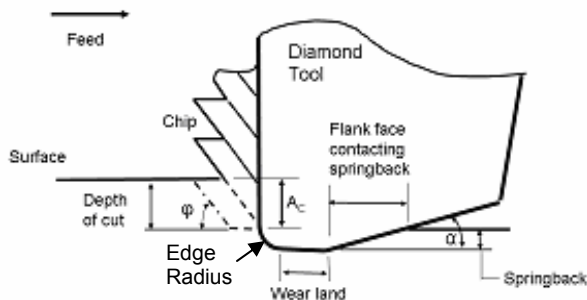


FIGURE 4. Friction contact regions of diamond tool used in tool force model, including components of $a_F(t)$: edge radius, wear land, and springback contact area.

For conventional diamond turning, the machining forces $F_C(t)$ and $F_T(t)$, the shear angle $\varphi(t)$, the uncut chip cross-section $a(t)$, and the friction area $a(t)$ are all constant. In the EVAM force model, these variables become functions of the tool position on the elliptical machining path, which in turn can be derived from the time-based kinematic functions (Equations 1,2).

Figure 5 shows conceptually the determination of the instantaneous uncut chip area $a_C(t)$ for the situation when $d/B < 1$ with discontinuous chips being produced. A round-nosed tool cutting a single groove is considered, but the method can be extended to other tool cross sections and to overlapping successive tool passes in the crossfeed direction. The sectional view in Figure 5 shows two consecutive tool passes and the change in the chip thickness along the centerline of the groove. On the preceding pass, a transient surface is created. The current pass makes a chip by cutting into the transient surface. The instantaneous chip thickness is the vertical separation between the two toolpaths at the same upfeed (horizontal) position for the region where the consecutive toolpaths overlap (Position 1). Otherwise the instantaneous chip thickness is the vertical distance between the workpiece surface and the toolpath (Positions 2, 3). In conventional machining the chip thickness is equal to the depth of cut, but it in EVAM the maximum chip thickness is less than or equal to the depth of cut. The oblique pictures of the tool rake face in Figure 5 show the instantaneous chip cross section area $a_C(t)$ for a round nosed tool at Positions 1, 2, and 3 indicated on the sectional side view.

Figure 6 shows a side view of the tool at the three positions on the toolpath from Figure 5. At Position 1 the tool is at the bottom of the elliptical tool path and frictional contact area $a_F(t)$ is at a maximum. It consists of the contact area associated with the cutting edge radius, the flank wear land behind the cutting edge, and the portion of the flank that contacts the just-cut work surface due to elastic springback. At Position 2 the tool is part way through the cutting pass, and $a_F(t)$ consists of the cutting edge radius and the flank wear land. At Position 3 the tool is about to exit the work material and $a_F(t)$ is only due to the edge radius.

Cerniway [2] provides mathematical details for calculating $a_C(t)$ and $a_F(t)$.

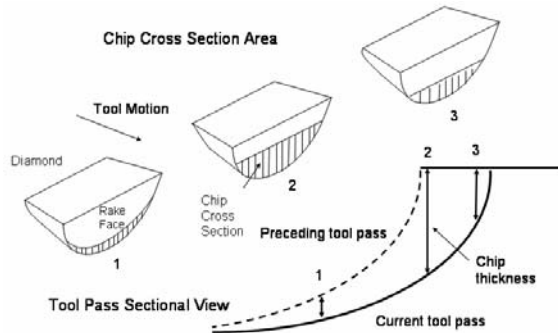


FIGURE 5. Chip formation at 3 points of tool pass. Chip thickness is established by the overlap between two successive elliptical tool passes.

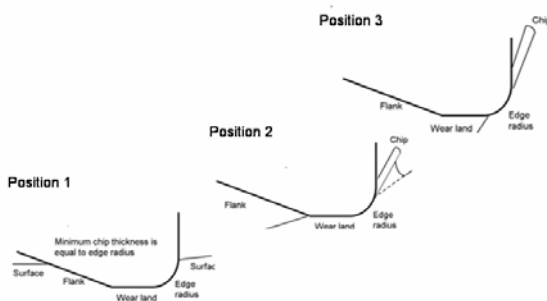


FIGURE 6. Reduction in friction contact area $a_f(t)$ as tool progresses through 3 different positions in elliptical cycle as shown in Figure 5.

It is apparent from Figure 6 that the instantaneous tool rake angle becomes increasingly negative as the tool proceeds along the elliptical path. Nakayama [5] and Dautzenburg [6] investigated shear angle formation due to rake angle geometry and material hardness. They determined that shear angle decreased with increasing negative rake angle, although comprehensive predictive models were not obtained. For EVAM force prediction, the instantaneous shear angle $\varphi(t)$ is assumed to be the bisector of the angle formed between the instantaneous rake angle, $\gamma(t)$ and the tool rake face. For a tool of zero nominal rake, this leads to $\varphi(t) = 45$ degrees when the direction of machining is horizontal, which is consistent with the shear angle for copper and aluminum under these conditions.

Work hardening of the material will take place when the depth of cut (or chip thickness in EVAM) is of the same order of magnitude as the tool edge radius [7]. If the instantaneous chip thickness falls within this work-hardened region the hardness H used in Equations 5-7 must be adjusted. The EVAM tool force model used

correction curves developed by Evans that varied the hardness according to the depth of cut and tool edge radius.

To estimate EVAM tool forces using the model, the basic procedure is: for time t , find the tool positions for the current and preceding passes. From this uncut chip thickness and cross section area $a_C(t)$, and the friction contact area $a_f(t)$ can be determined. Next the instantaneous tool rake angle is found, and from it the shear angle $\varphi(t)$. Finally the instantaneous material hardness H is found. These instantaneous values are inserted into Equations 5, 6, and 7 to estimate the cutting force and thrust forces at time t . The machining forces can be calculated at multiple points to construct curves showing the variation throughout an elliptical vibration cycle. The average forces can be estimated by numerically integrating forces throughout a complete cycle and dividing by the cycle period.

PREDICTED AND MEASURED EVAM TOOL FORCES

Cerniway [2] and Negishi [3] investigated EVAM tool forces for a range materials, vibration frequencies, tool conditions, and depths of cut. The EVAM model described in the preceding section was used to predict thrust and cutting forces. Cerniway used a prototype low-frequency version of the Ultramill ($f < 400$ Hz), while Negishi used a next-generation model at frequencies of 1 to 4 KHz. In both cases machining forces were measured by a 3-axis load cell installed between the vacuum chuck of the diamond turning machine and the workpiece. This sensor location gave a natural frequency for the measurement loop of 12.5 KHz, considerably greater than if the load cell were installed between the Ultramill and the tool post. If the EVAM frequency is near the measurement loop's natural frequency then the force values will be distorted by resonance effects, while if it is significantly larger than the measurement loop natural frequency the force measurement will be attenuated and artificially low values obtained. Negishi found that when machining with a frequency of 4 KHz there was significant distortion in the force signal from the measurement loop vibrations being unable to die out between EVAM cycles, but at 1 KHz distortion was minimal.

Cerniway conducted groove-cutting experiments at 10 Hz in C1100 copper to compare measured and predicted EVAM machining forces. The

vibration ellipse amplitudes were $47.5 \mu\text{m} \times 7.3 \mu\text{m}$ ($A \times B$) and the depth of cut was $6 \mu\text{m}$ ($d/B = 0.82$). The tool had zero rake and a nose radius of 3 mm. Representative results are shown in Figures 7, 8, and 9. These figures plot the predicted and measured EVAM machining forces for the portion of the cycle during which the tool is cutting. Figure 7 and 8 show the effect of changing duty cycle. In these plots the tool is considered to be “worn” with an estimated edge radius of 300 nm. In Figure 7 the duty cycle is 25%, which gives a maximum chip thickness equal to the depth of cut. In this case peak EVAM cutting force is 46% of the predicted conventional cutting force, while peak EVAM thrust force is 73% of the predicted conventional thrust force. In Figure 8, the duty cycle is 23%. The peak EVAM cutting force is only 30% of the the conventional cutting force, and the peak EVAM thrust force is 64% of the conventional thrust force. This reduction in peak EVAM force as duty cycle grows smaller is mainly due to the reduction in maximum chip thickness and chip cross section $a_C(t)$ caused by the closer spacing of overlapping elliptical tools passes at the smaller duty cycle. Since the tool is worn, the friction contact area $a_F(t)$ is large relative to $a_C(t)$, and is the reason why the EVAM thrust force decreases less rapidly than the EVAM cutting force.

Figures 8 and 9 show the effect of tool wear condition, for the same machining parameters and a 23% duty cycle. In Figure 9 the tool is “sharp” with an estimated edge radius of 40 nm, while the tool in Figure 8 is “worn” (300 nm edge radius). The peak EVAM cutting force for the sharp tool is 33% of the peak worn tool EVAM cutting force (and 21% of the predicted conventional sharp tool cutting force). The peak EVAM sharp tool thrust force is 21% of the peak EVAM thrust force with a worn tool (37% of the conventional sharp tool thrust force). With the sharp tool the friction contact area $a_F(t)$ in Equations 5 and 6 becomes very small, and tool forces are essentially established by the chip thickness and cross section area $a_C(t)$.

In Figures 7 thru 9 the measured EVAM machining forces are seen to be in good agreement with forces predicted by the model. Cerniway also conducted EVAM groove cutting tests in 6061-T6 aluminum and 1018 steel. Frequency, machining ellipse, and depth of cut were the same as for the copper tests described above. A “worn” tool was used in these tests.

Table 1 shows peak measured EVAM tool forces when machining these materials, along with associated C1100 copper results. For all

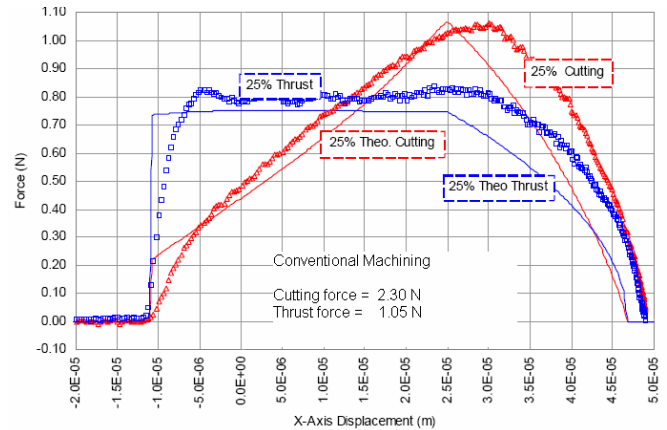


FIGURE 7. Predicted and measured EVAM tool forces at 25% duty cycle. C1100 copper, $f = 10 \text{ Hz}$, depth of cut = $6 \mu\text{m}$. Worn tool.

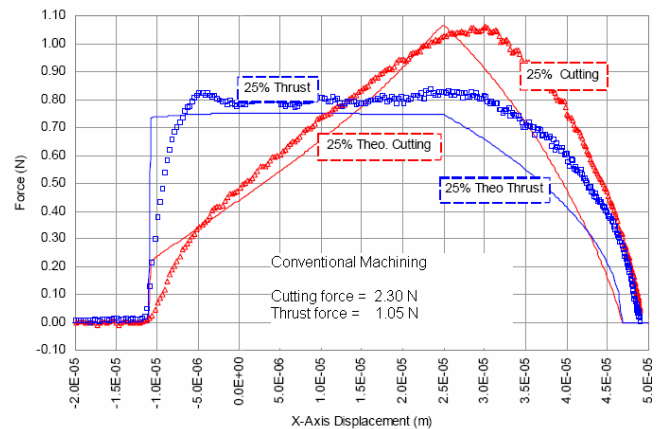


FIGURE 8. Predicted and measured EVAM tool forces at 23% duty cycle. C1100 copper, $f = 10 \text{ Hz}$, depth of cut = $6 \mu\text{m}$. Worn tool.

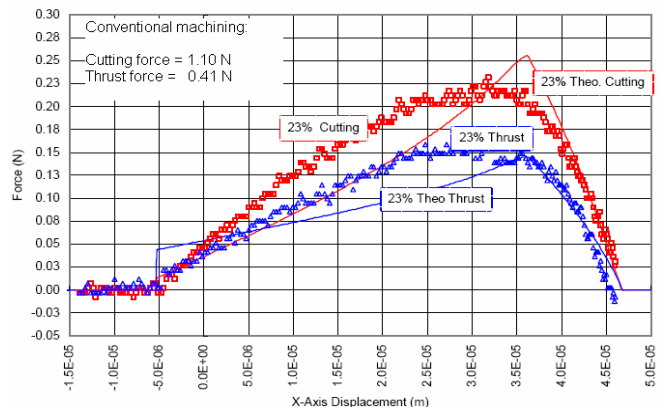


FIGURE 9. Predicted and measured EVAM tool forces at 23% duty cycle. C1100 copper, $f = 10 \text{ Hz}$, depth of cut = $6 \mu\text{m}$. Sharp tool.

TABLE 1: Measured EVAM Machining Forces

Duty Cycle	C1100 Copper		6061-T6 Aluminum		1018 Steel	
	E 123 GPa H 0.84 GPa		E 69 GPa H 0.88 GPa		E 205 GPa H 1.57 GPa	
	C	T	C	T	C	T
	[N]	[N]	[N]	[N]	[N]	[N]
22 %	0.40	0.67	0.48	0.88	0.70	1.21
23 %	0.70	0.71	0.83	0.93	1.23	1.28
25 %	1.05	0.83	1.26	1.09	1.85	1.49
Conv cutting	2.44	1.29	2.51	1.52	3.82	2.00
Machining conditions: $f = 10$ Hz Ellipse = $47.5 \mu\text{m} \times 7.3 \mu\text{m}$ ($A \times B$) Depth of Cut, $d = 6 \mu\text{m}$ $d/B = 0.82$						
Tool: Nose radius = 3mm Edge radius ~ 300 nm (worn)						

Notes: "C" = cutting force "T" = thrust force
 H is Vickers hardness

materials EVAM cutting forces are reduced to 20-50% of the conventional cutting force, and EVAM thrust forces to 60-75% of the conventional thrust force, depending on the duty cycle.

Negishi performed single-groove cutting experiments in 6061 aluminum at 1 KHz. The vibration ellipse amplitudes were $20 \mu\text{m} \times 4 \mu\text{m}$ ($A \times B$). The tool had zero rake angle and a nose radius of $500 \mu\text{m}$. Predicted and measured EVAM machining forces were compared for 4 different depths of cut and were within 5%. Figure 10 shows tool forces in the cutting portion of the machining cycle for when depth of cut was $8.9 \mu\text{m}$ ($d/B = 2.2$). In this case a continuous chip was produced due to the depth of cut being greater than the ellipse vertical amplitude.

These results do not show the thrust force reversal reported by Moriwaki and Shamoto (see Figure 1). Cerniway attributed this to their machining at $d/B \approx 3$, creating a continuous chip that remains attached to the workpiece. The thrust reversal is explained as being caused by the tool interacting with the overhanging chip during the portion of the cycle that the rake is out of contact with the uncut material. This argument appears to be invalidated by Negishi's result for a similar value of d/B (Figure 10). One difference between the processes is that the Moriwaki-Shamoto tool vibrates in a nearly-circular path while the Ultramill uses a highly-eccentric ellipse with the

face

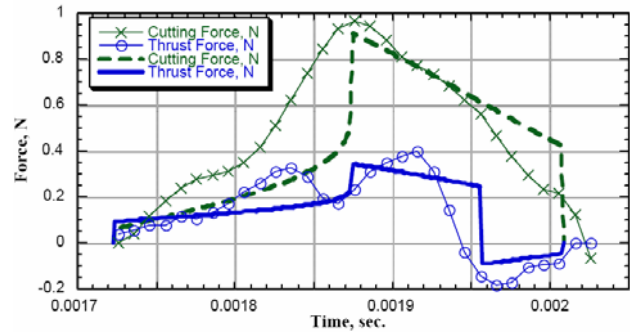


FIGURE 10. Predicted and measured EVAM tool forces at 1000 Hz when cutting 6061 aluminum. Depth of cut = $8.9 \mu\text{m}$, ($d/B=2.2$), 25% duty cycle.

parallel to the upfeed direction. The conflict remains unresolved.

CONCLUSIONS

1. A tool force model was developed for EVAM, derived from an existing model for conventional diamond turning. Instantaneous chip cross-section, and contact area behind the rake face are determined as a function of the tool position in the elliptical machining path. Material shear angle is varied to reflect the changing tool rake angle. Work hardening effects are included.

2. Machining tests were conducted in copper, aluminum, and steel. Depending on machining conditions, peak EVAM cutting forces were 20-50%, and peak EVAM thrust forces were 60-75% of the values for conventional machining. Good agreement was obtained between experimental results and predictions by the force model.

REFERENCES

- [1] Shamoto, E., Moriwaki, T., "Study on Elliptical Vibration Cutting", 1994, *CIRP Annals*, v43:1
- [2] Cerniway, M., "Elliptical Diamond Milling: Kinematics, Force, and Tool Wear", MS thesis, NCSU, 2001
- [3] Negishi, N., "Elliptical Vibration-Assisted Machining with Single Crystal Diamond Tools", MS thesis, NCSU, 2003
- [4] Arcona, C., "Tool Force, Chip Formation and Surface Finish in Diamond Turning", PhD dissertation, NCSU, 1996
- [5] Dautzenberg, J., Hijink, J., Van der Wolf, A., "The Minimum Energy Principle Applied to the Cutting Process of Various Workpiece Materials and Tool Rake Angles", *CIRP Annals*, v31:1m 1982
- [6] Nakayam, K., Minoru, A., Torahiko, K., "Machining Characteristics of Hard Materials", *CIRP Annals*, v37:1, 1988
- [7] Dresher, J., "Tool Force, Tool Edge, and Surface Finish Relationships in Diamond Turning", PhD dissertation, NCSU, 1991